A&A manuscript no.
(will be inserted by hand later)

Your thesaurus codes are:
09.09.01: ρ Oph, 09.04.01, 13.09.2, 13.09.3, 13.09.4

ASTRONOMY
AND
ASTROPHYSICS
17.9.1996

Letter to the Editor: first results from ISO

Mid-Infrared Imaging Spectroscopy in Ophiuchus

F. Boulanger[1], **W. T. Reach**[1], **A. Abergel**[1], **J.P. Bernard**[1], **C. J. Cesarsky**[2], **D. Cesarsky**[1], **F.X. Désert**[1], **E. Falgarone**[3], **J. Lequeux**[3], **L. Metcalfe**[4], **M. Pérault**[3], **J.L. Puget**[1], **D. Rouan**[5], **M. Sauvage**[2], **D. Tran**[2], **and L. Vigroux**[2]

[1] Institut d'Astrophysique Spatiale, Université Paris XI, France
[2] Service d'Astrophysique, CEA, Saclay, France
[3] DEMIRM, Observatoire de Paris et Ecole Normale Supérieure, France
[4] ESA, Villafranca del Castillo, Spain
[5] DESPA, Observatoire de Meudon, France

Received July 16, 1996; accepted September 6, 1996

Abstract. The dust emission spectrum between 5 and 16 μm has been measured at the northern edge of the dense cloud in Ophiuchus at a position where the radiation field intensity is estimated to be 10-20 times the mean Solar neighborhood value. The spectrum shows the well known emission bands at 6.2, 7.7, 8.6, 11.3 and 12.7 μm. ISO allows to detect the emission features for a radiation field intensity two orders of magnitude smaller than in the objects previously observed. Since all of these bands are considered to be characteristic of C-C or C-H bonds in aromatic hydrocarbons this observation strongly supports the existence of large aromatic molecules in the general interstellar medium. An important result of the observation is the presence of a significant continuum below the features at all wavelengths, and in particular, a featureless continuum between the 8.6 and 11.3 μm features and beyond that at 12.7 μm. The Ophiuchus spectrum is remarkably similar to that measured in NGC 7023. We argue that both the bands and the continuum emission must come from molecules or small aggregates with less than a few hundred carbon atoms.

Key words: infrared:general-ISM:lines and bands, continuum; ISM:general- dust,extinction-individual:ρ Oph

1. Introduction

Near and mid-IR observations of the Galactic plane and reflection nebulae (Andriesse 1978, Sellgren et al. 1985) have led to the discovery of interstellar particles small enough to be heated to high temperatures by the absorption of single photons. By providing extensive data on the mid-IR emission from interstellar matter in various environments, the Infrared Astronomical Satellite (IRAS) demonstrated the ubiquity and importance of these small particles. Léger and Puget (1984) associated small particles with the presence of a well defined set of emission bands at 3.3, 6.2, 7.7, 8.6 and 11.3 μm in the spectra of a wide range of celestial objects. These emission bands being characteristic of C-C and C-H bonds in aromatic molecules, they proposed that the smallest particles are large polycyclic aromatic hydrocarbons (PAHs). Since this hypothesis was put forward, spectral data have been gathered on bright compact objects; however, before the launch of the Infrared Space Observatory (ISO, Kessler et al. 1996), little spectral information was available on the diffuse emission from interstellar matter away from hot stars. Since various observations show signs of the destruction of small particles in strong UV fields, the relevance of existing spectral observations to the general ISM have always been questionable. Balloon observations of the Galactic plane in narrow-band filters clearly indicate the presence of the 3.3 and 6.2 μm emission features in the spectrum of the diffuse emission from the Galaxy (Giard et al. 1994, Ristorcelli et al. 1994).

We present here the first result of a guaranteed time project of the ISO camera (ISOCAM, Cesarsky et al. 1996a) team to study emission properties of small particles in various environments and in particular in regions of low heating.

Send offprint requests to: F. Boulanger

2. Observations and Data Reduction

The observations presented in this paper were made on the 18th of February 1996. ISOCAM was pointed at right ascension $16^h22^m40.1^s$ and declination -24°00′00″ (1950). The ecliptic coordinates $\lambda = 247.87°$ and $\beta = -2.40°$ and the solar elongation 80° are important parameters because a significant fraction of the measured flux is zodiacal light from interplanetary dust heated by the Sun. A complete scan of the long-wavelength circular variable filters (CVF) was performed towards this position. The 12″ pixel field of view lens was used to maximize the flux on each pixel. Since the stabilization time of the LW detector of ISOCAM is inversely proportional to the received flux, the higher illumination greatly reduces the effects of detector instability. The two long wavelength CVFs were scanned going down in wavelength: first the LW-CVF2 from 16.6 to 9.0 μm and second the LW-CVF1 from 9.4 to 5.0 μm. At each CVF step, 12 frames of 2.1 sec were taken for a total observing time of 4200 sec. The spectral resolving power of LW-CVF1 goes up from 37 at 5.0 μm to 43 at 9.0 μm, that of LW-CVF2 from 35 at 9.0 μm to 48 at 16.0 μm.

The complete set of images was put into a cube and temporally filtered to remove glitches due to cosmic rays. The images at a given wavelength were spliced together using the LW-CVF1 data up to 9.2 μm and the LW-CVF2 down to 9.2 μm with no adjustment, leading to a cube of images with 146 independent spectral points. A stabilized dark obtained during calibration time was subtracted from each image. We used the algorithm presented by Abergel et al. (1996) to estimate and correct for gain drifts along the observation. The corrections were found to be small ($<$ 5%) over most of the spectrum except at the beginning of the observation ($\lambda > 16$ μm) and for the 6.2 μm emission feature, for which the contrast was increased by 15% by the gain correction. Since the gain corrections obtained for the beginning of the observation depend on previous data to which we do not have access, data at $\lambda > 16$ μm should be considered with caution.

Flat-fielding is a critical step, because the lens used to obtain 12″ pixel-field-of-view only illuminates the central 16×16 pixels of the array, with significant vignetting. We have used an observation made with the same optical configuration on a field free of interstellar cirrus to flat-field the images. We have used the same flat at all wavelengths.

The spectral response of the detectors was calibrated using the ratio of observed to model spectrum of HD 185395, an F type main sequence star. Comparison between the spectral observations of three calibration stars show that the relative spectral response is presently known to better than 5%. The absolute calibration of ISOCAM for extended sources has been checked by comparing measurements of the zodiacal light with those made with the Diffuse Infrared background Experiment (DIRBE, Boggess et al. 1992). A general description of ISOCAM and the calibration is presented by Cesarsky et al. (1996a).

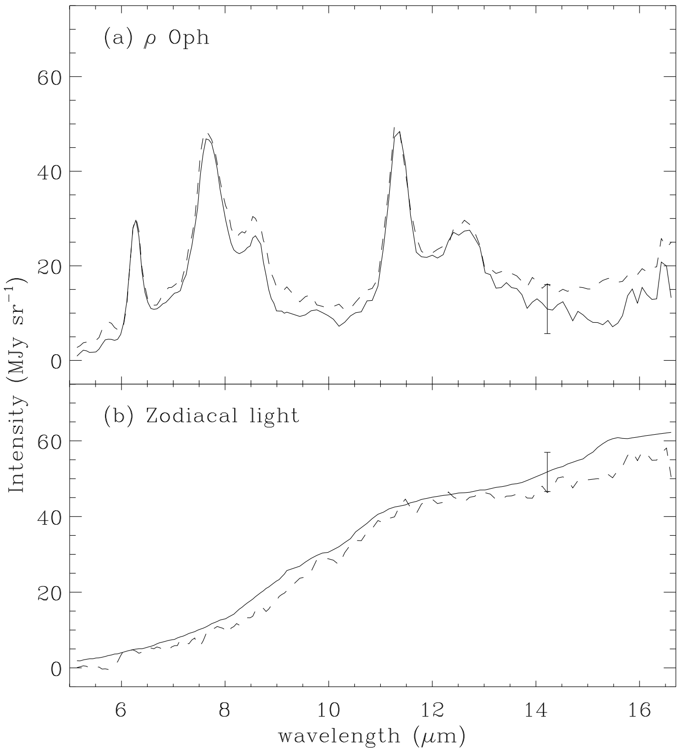

Fig. 1. Mean Emission Spectrum within the ρ Oph field. The solid line is the spectrum derived from data averaging, the dashed line that resulting from the correlation analysis (Sect. 3.3). The difference between the two spectra corresponds to a 10% difference in the zodiacal light subtracted from the data (bottom panel). The error bar at long wavelengths represents ±10% variations in the continuum associated with the zodiacal light subtraction.

3. Mid-IR emission spectrum

3.1. Physical Conditions

Among nearby clouds, the Ophiuchus cloud is remarkable for a high degree of gas concentration and a high star formation activity. The position selected for spectro-imaging observations is at the North-Western corner of the large Ophiuchus map presented by Abergel et al. (1996). With IRAS data, Bernard et al. (1993) have shown that the 12/100 μm emission ratio is enhanced at the cloud edge, where the ^{13}CO emission drops. The observed position is within the halo of enhanced 12 μm emission on the northern side of the cloud, 40′ south of the stars ρ Oph A and B. The infrared emission on the northern side of the cloud is consistent with the idea that this cloud edge is heated by one or both of the B2 stars ρ Oph A and B. Bernard et al. combined the IRAS data with estimates of the gas column density to derive the cloud to star distance. Using their results we find that the observed position is located at 3.2 pc from ρ Oph. For a star luminosity of $L = 2.5\ 10^4\ L_\odot$ we get an estimate of the radiation field, G = 10 in units of the mean Solar neighborhood radiation field. From the integrated ^{13}CO(1-0) emission (4.7 $\mathrm{K\,km\,s^{-1}}$) at the position of the CAM observation, we estimate the gas column density $N_H \sim 1\ 10^{22}\,\mathrm{cm^{-2}}$, based on the $N(^{13}CO)/A_v$ relation derived by Frerking et al. (1982). The 100 μm brightness at the observed position is 400 MJy/sr. These two numbers, when compared to the calculations of Bernard et al. (1993) (see their Fig. 9), also lead to a value of G in the range 10-15. By dividing the column density by the diameter of the Ophiuchus cloud (1.5 pc) we derive an estimate of the gas density, $n_H \sim 2 \times 10^3\mathrm{cm^{-3}}$.

3.2. Mean Emission Spectrum

The mean emission spectrum over the field was first derived by averaging the central 12×12 pixels. The zodiacal contribution to this spectrum was estimated in the following way. We assumed that the spectral shape of the zodiacal emission in the direction of Ophiuchus is the same as that measured at another position close to the ecliptic plane (Reach et al. 1996). The intensity of the zodiacal light depends on the ecliptic coordinates and the solar elongation. Observations with the DIRBE on board of the Cosmic Background Explorer (COBE) provide a complete data base of sky measurements over the whole sky for the whole range of solar elongations permitted for ISO observations (60 to 120°). We thus used the DIRBE data to estimate the ratio of zodiacal emission between the Ophiuchus and Reach et al. observations. The zodiacal light contribution in the Ophiuchus data was then computed to be the Reach et al. spectrum times the emission ratio derived from DIRBE data. The main weakness of this method for removing the zodiacal light is to rely on the equality of the detector response between the two observations.

The solid-line spectrum presented in Fig. 1 is the difference between the mean spectrum and the estimated zodiacal light. The noise in the spectrum roughly scales with the total brightness because it is related to gain variations. Uncertainty on the dark current affects the absolute level at 5μm. The spectrum shows spectacularly the major emission bands at 6.2, 7.7, 8.6 and 11.3 μm which have been previously observed in many objects such as reflection nebulae, HII regions and planetary nebulae. The emission band at 12.7 μm had been seen in a few objects (Witteborn et al. 1989) and in particular for the interstellar medium in Orion (Roche et al. 1989). We are confident that the small bumps at 5.2 and 5.6μm are true detections of the weak features discovered by Allamandola et al. (1989). All of these lines are considered to be characteristic of C-C or C-H bonds in aromatic hydrocarbons. The new ISO observations enable us to detect the emission features in an environment where the radiation field is at least two orders of magnitude smaller than in the objects previously observed. Due to uncertainties on the gain correction at the beginning of the observation (Sect. 2) we are not confident of the emission rise seen at the long wavelength end of the spectrum but it may be real.

An important result of the observations is the existence of a significant continuum below the features at all wavelengths, and in particular, a featureless continuum between the 8.6 and 11.3 μm features and beyond the 12.7 μm band. The presence of continuum emission in the near, mid-IR emission from interstellar matter is also demonstrated by the detection of interstellar emission in the M band (4.9 μm) sky maps made with the DIRBE data (Bernard et al. 1994). We have decomposed the spectrum of Figure 1 by fitting the features with gaussians and the continuum with a second order polynomial. The results of this decomposition are summarized in Table 1; the last line of the Table represents the total emission integrated from 5 to 16 μm. Because the features all lie on top of broad structures, the separation of the emission between continuum and features is somewhat arbitrary, and the formal error bars listed in the Table underestimate the true uncertainties on the band parameters. If we sum the band intensities given in the Table, we find that the features account for only $\sim$ 30% of the integrated emission measured from 5 to 16 μm. We convolved the Ophiuchus spectrum with the IRAS 12 μm filter and found that $\sim$ 60% of the IRAS in-band brightness comes from the continuum. Also, for comparison with other data, the ratio $I_\nu(6.75\mu\mathrm{m})/I_\nu(15\mu\mathrm{m})$ derived from observations in the often used LW2 and LW3 filters is 1.1 at the position of the CVF observation.

Table 1. Spectral Features toward ρ Oph

wavelength (μm)	brightness ($\mathrm{MJy\ sr^{-1}}$)	width (μm)	Intensity $\mathrm{Wm^{-2}sr^{-1}}$
6.280 ± 0.004	23.1 ± 0.7	0.18 ± 0.01	$3.5 10^{-7}$
7.705 ± 0.004	37.5 ± 0.4	0.48 ± 0.01	$9.7 10^{-7}$
8.549 ± 0.008	16.7 ± 0.5	0.35 ± 0.02	$2.5 10^{-7}$
11.342 ± 0.004	36.5 ± 0.8	0.31 ± 0.01	$2.7 10^{-7}$
12.504 ± 0.022	15.8 ± 0.4	1.02 ± 0.04	$3.2 10^{-7}$
Total Power		5-16μm	$7.0 10^{-6}$

3.3. Spatial Structure

In the previous section, the Ophiucus spectrum is derived from a combination of two observations for which the detector is assumed to have the same response. This leaves some uncertainty on the zodiacal subtraction, which could affect the level of continuum emission. We present here an

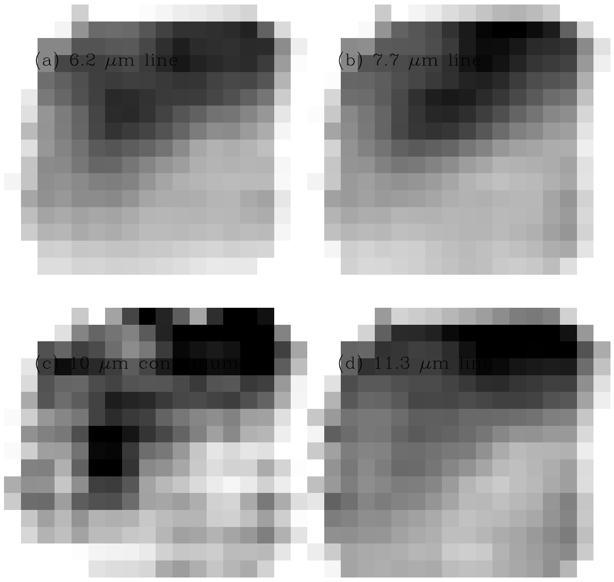

Fig. 2. Sample of four images showing within the 3'x3' field of view the spatial distribution of 6.2, 7.7 and 11.3μm band emission (a,b,d), and that of the continuum at 10μm (c). White pixels correspond to flagged pixels. The brightest regions are white. The gray-scale dynamic range for the 4 images is $\pm 30\%$ of their mean brightness.

alternative method to derive the ρ Oph spectrum which does not suffer from this uncertainty.

Sample images of the structure within the ISOCAM field are shown in Fig. 2. The zodiacal light may be considered uniform over the field, and the structure is related to interstellar emission. By correlating this spatial structure between wavelengths one may separate the two sources of emission. We assumed that the emission over the camera field fo view could be expressed as $I_\nu(x,y) = Z_\nu + G_\nu g(x,y)$ where x and y represent spatial coordinates. For the Galactic template $g(x,y)$ we used the map of the intensity of the 7.7 μm feature above the adjacent continuum. Each spectral image was linearly correlated with this template. The results of the correlation are the slope, G_ν, which is the Ophiuchus spectrum, and the intercept for zero interstellar emission, Z_ν, which is the zodiacal light spectrum. These two spectra are plotted in Fig. 1 with dashed lines. The two Ophiuchus spectra derived in independent ways are very similar; the difference between the two essentially corresponds to a 10% difference in the amount of zodiacal light subtracted. The zodiacal spectrum derived from the correlation analysis matches well in spectral shape that of Reach et al. The 10% intensity difference is within the range of observed variations in the detector response from observation to observation (Cesarsky et al. 1996a). We consider this 10% difference in the zodiacal light intensity as the uncertainty on the continuum level of the Ophiuchus spectrum. This uncertainty is marked with an error bar in the plot. Uncorrected response drifts within the observation could also affect the continuum level. Existing calibration observations allow us to be confident that associated errors are within the 10% error bar.

4. Discussion

In this first series of ISO papers, results from ISOCAM spectral imaging observations are presented for two additional Galactic objects: the reflection nebula NGC 7023 and the HII region/molecular cloud interface M17 (Cesarsky et al. 1996b,c). With these observations we can already put the Ophiuchus results into a broader context. The Ophiuchus spectrum is very similar to those measured in NGC 7023. In both Ophiuchus and NGC 7023 we are looking at matter at the edge of a dense cloud illuminated by a hot non-ionizing star with the difference that the radiation field intensity is in Ophiuchus two to three orders of magnitude smaller than in NGC 7023. It is remarkable that the emission spectrum remains so similar despite this large change in radiation intensity. It is only in M17, where the radiation field is 4 to 5 orders of magnitude stronger than in Ophiuchus (Cesarsky et al. 1996c, Verstraete et al. 1996), that the intensity of the continuum sharply increases with increasing wavelengths. For both Ophiuchus and NGC 7023, the radiation field is too low to expect significant contribution to the observed emission from small grains heated by the combined heating of multiple photons.

A spectrum independent of the radiation field intensity is a basic characteristic of emission from particles heated by one photon at a time. After absorption of a photon, a small particle is heated to a high temperature and emits most of its energy near that peak temperature, because the heat capacity is a steeply increasing function of temperature. There is thus a rough correspondence between particle size and emission wavelength (Puget and Léger 1989) which can be used here to estimate that the particles accounting for the observed emission should on average contain about 100 carbon atoms. This should apply both to the bands and the continuum. Within the framework of the Désert et al. (1990) model and for the radiation field at the ρ Oph position, we checked that most of the emission in the 5–16 μm range comes from particles smaller than a few 100 carbon atoms. Larger particles do not get hot enough to contribute significantly.

A main question raised by the Ophiuchus observations is that of the origin of the continuum emission. The continuum seems concentrated around the emission features from aromatic hydrocarbons and its intensity is correlated with that of the bands. Both facts suggest that the particles emitting the continuum emission are the same, or at least closely related, to those emitting the bands. Laboratory spectra of PAHs show numerous lines other than the main astronomical features. Moutou et al.(1996)

have recently presented a composite spectrum, combining the absorption spectra of many PAHs. The line crowding in this spectrum suggests that the continuum emission could actually be the added contributions of weak features with wavelengths that depend on the particular molecules. Within this interpretation, the emission bands could represent accumulation points of the main bands. For example, the position of the CH out of plane bending mode varies from 11 to 15μm depending on the number of H atoms on the aromatic rings (Witteborn et al. 1989). It is thus not surprising to see significant emission around the 11.3 and 12.7 μm bands and in particular at longer wavelengths. The particles responsible for the astronomical emission are also larger than the molecules studied in the laboratory and they may be clusters of a few molecules. Their optical properties could be in between those of isolated molecules and those of amorphous carbon. Additional laboratory experiments and quantum calculations especially for large molecules and small carbon clusters are clearly needed to clarify the nature of the emitting particles.

Acknowledgements. Based on observations with ISO, an ESA project with instruments funded by ESA Member States (especially the PI countries: France Germany, the Netherlands and the United Kingdom) and with the participation of ISAS and NASA.

References

Abergel, A. et al. 1996, A& A this issue
Allamandola, L. J., Bregman, J. D., Sandford, S. A., Tielens, A. G. G. M., Witteborn, F. C., Wooden, D. H., Rank, D. 1989, Ap. J. 345, L59
Andriesse, C.D. 1978, A& A 66, 169
Bernard, J.P., Boulanger, F., Puget, J.L. 1993, A& A 277, 609
Bernard, J.P., Bernard, F., Désert, F. X., Giard, M., Helou, G., Puget, J. L. 1994, A& A 291, L5
Boggess, N.W. et al. 1992, Ap. J. 397, 420
Cesarsky, C.J. et al. 1996a, A& A this issue
Cesarsky, D., Lequeux, J., Abergel, A., Perault, M., Palazzi, E., Madden, S., Tran, D. 1996b, A& A this issue
Cesarsky, D., Lequeux, J., Abergel, A., Perault, M., Palazzi, E., Madden, S., Tran, D. 1996c, A& A this issue
Désert F.X., Boulanger, F. and Puget, J.L. 1990, A& A 237, 215
Frerking, M.A., Langer, W.D., Wilson, R.W. 1982, Ap. J. 262, 590
Giard, M., Lamarre, J. M., Pajot, F., Serra, G. 1994, A& A 286, 203
Kessler, M. et al. 1996, this issue
Léger, A., and Puget J.L. 1984, A& A 137, L5.
Moutou, C., Léger, A., d'Hendecourt, L. 1996, A& A 310, 297
Puget, J.L. and Léger, A. 1989, ARA& A 27, 161
Reach W.T. et al. 1996, A& A this issue
Ristorcelli, I., Giard, M., Meny, C., Serra, G., Lamarre, J. M., Le Naour, C., Leotin, J., Pajot, F. 1994, A& A 286, L23
Roche, P.F., Aitken, D.K., Smith, C.H. 1989, MNRAS 236, 485
Sellgren, K., Allamandola, L.J., Bregman, J.D., Werener, M.W., Wooden, D.H. 1985 Ap.J. 299, 416
Verstraete, L. et al. 1996, A& A, this issue
Witteborn, F. C., Sandford, S. A., Bregman, J. D., Allamandola, L. J., Cohen, M. 1989, Ap. J. 341, 270

This article was processed by the author using Springer-Verlag LaTeX A&A style file *L-AA* version 3.